SWCNT Networks on Nanoporous Silica Catalyst Support: Morphological and Connectivity Control for Nanoelectronic, Gas-Sensing, and Biosensing Devices

Zhao Jun Han,[†] Hamid Mehdipour,[†,‡] Xiaoguang Li,[†,§] Jun Shen,[§] Lakshman Randeniya,[†] Hui Ying Yang,[∥] and Kostya (Ken) Ostrikov[†,‡,*]

[†]Plasma Nanoscience Centre Australia (PNCA), CSIRO Materials Science and Engineering, P.O. Box 218, Lindfield, New South Wales 2070, Australia, [‡]Complex Systems, School of Physics, The University of Sydney, Sydney, New South Wales 2006, Australia, [§]Shanghai Key Laboratory of Special Artificial Microstructure Materials and Technology, Tongji University, Shanghai, P. R. China, and [∥]Singapore University of Technology and Design, 20 Dover Drive, 138682, Singapore

ABSTRACT Effective control of morphology and electrical connectivity of networks of single-walled carbon nanotubes (SWCNTs) by using rough, nanoporous silica supports of Fe catalyst nanoparticles in catalytic chemical vapor deposition is demonstrated experimentally. The very high quality of the nanotubes is evidenced by the G-to-D Raman peak ratios (>50) within the range of the highest known ratios. Transitions from separated nanotubes on smooth SiO_2 surface to densely interconnected networks on the nanoporous SiO_2 are accompanied by an almost two-order of magnitude increase of the nanotube density. These transitions herald the hardly detectable onset of the nanoscale connectivity and are confirmed by the microanalysis and electrical measurements. The achieved effective nanotube interconnection leads to the dramatic, almost three-orders of magnitude decrease of the SWCNT network resistivity compared to networks of similar density produced by wet chemistry-based assembly of preformed nanotubes. The growth model, supported by multiscale, multiphase modeling of SWCNT nucleation reveals multiple constructive roles of the porous catalyst support in facilitating the catalyst saturation and SWCNT nucleation, consistent with the observed higher density of longer nanotubes. The associated mechanisms are related to the unique surface conditions (roughness, wettability, and reduced catalyst coalescence) on the porous SiO_2 and the increased carbon supply through the supporting porous structure. This approach is promising for the direct integration of SWCNT networks into Si-based nanodevice platforms and multiple applications ranging from nanoelectronics and energy conversion to bio- and environmental sensing.

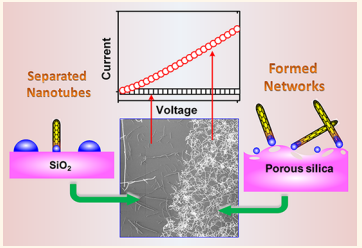

KEYWORDS: single-walled carbon nanotubes · nanonetworks · nanoscale electrical connectivity · porous catalyst support · graphene layer

Single-walled carbon nanotubes (SWCNTs) are one-dimensional nanomaterials with unique electrical, thermal, mechanical, and optical properties.[1] SWCNT networks, which consist of interconnected randomly oriented or aligned nanotubes,[2,3] have many advantages in nanodevice applications compared to assemblies of individual nanotubes, such as long-term stability, reproducibility, scalability, and low cost.[4] This makes the SWCNT networks (SWCNTNs) among the most attractive materials for applications ranging from thin-film transistors (TFTs), transparent conducting layers, photovoltaic solar cells, to biosensors and drug/protein/gene delivery systems.[5−8]

Among a variety of structural and morphological parameters, the nanotube density is the key factor that determines the network performance. For example, by varying the nanotube density, one can optimize the optical transparency and electrical resistivity in nano- and optoelectronic applications.[4,9] Performance of SWCNTN-based TFTs and biosensors have also been intimately related to the nanotube density.[2,10] However, higher nanotube densities do not necessarily lead to better device performance as the primary factor is the nanoscale electronic connectivity within the networks.[11] The morphological and connectivity factors are thus strongly interlinked, yet it remains largely unknown which SWCNT network arrangements yield the optimum electrical conduction.

The electron transport through the networks is determined by the nanotube−nanotube and nanotube−metal interactions.[12,13] In networks of randomly oriented SWCNTs, a high intertube contact resistance and a low carrier mobility are expected because of the strong electron scattering and high Schottky barriers. Conversely, when the nanotubes are aligned or the network morphology is optimized, much higher electrical conductance and carrier mobility can be achieved.[14,15]

The SWCNT networks are commonly fabricated by sophisticated processes based on

* Address correspondence to kostya.ostrikov@csiro.au.

Received for review December 19, 2011 and accepted June 10, 2012.

Published online June 10, 2012
10.1021/nn302020a

wet chemical processing, catalytic chemical vapor deposition (CCVD), or combinations thereof. Although wet chemical processing (*e.g.,* spray coating, spin coating, Langmuir–Blodgett process, vacuum filtration, inkjet printing, *etc.*) offer reasonable control over the SWCNTN density, the nanotubes are often shortened and otherwise damaged due to the adverse effects of surfactants, chemicals, and sonication.[16,17] In contrast, CCVD can produce large-scale SWCNT networks and preserve the intrinsic nanotube properties. However, the ability to tailor the density, morphology, and connectivity of the networks without compromising the structural quality of the nanotubes still remains a major challenge in CCVD, mostly because of the many process parameters (*e.g.,* catalyst, temperature, gas, and pressure) that affect the SWCNT nucleation and growth.[18−23] Direct integration of SWCNTNs into the presently dominant Si-based nanodevice platform is also a significant issue because of the frequently observed uncontrollable coalescence of metal catalyst nanoparticles (CNPs) on smooth Si substrates under high-temperature conditions of SWCNT synthesis.[24]

Here we show experimentally that the above challenges can be resolved by a simple approach wherein porous silica is used as a Fe CNP support. Not only is the nanotube density increased by nearly 2 orders of magnitude but also the SWCNTs become much longer compared to different cases when smooth SiO_2 layers were used as catalyst supports. This in turn enables effective nanoscale connectivity and dramatically reduces the electrical resistivity of the networks. A special "knotted" morphology is achieved while preserving a very high structural quality of the nanotubes; these factors lead to the significantly improved electron transport through the networks. The proposed growth model relates these features to the interactions between the catalyst and the nanoporous SiO_2 (np-SiO_2) support, which are studied using multiscale, multiphase modeling of the SWCNT nucleation and growth. It is shown that the unique conditions (*e.g.*, surface energy, wettability, and carbon supply) offered by the rough surface and the nanoporous interior of the np-SiO_2 layer indeed lead to denser and longer nanotubes. In addition, sensor devices fabricated using our SWCNT networks show excellent performance in the detection of NH_3 and NO_2 gases as well as prostate specific antigen (PSA) cancer biomarker molecules. These results contribute to the ultimately deterministic CCVD growth of SWCNT networks for high-performance nanodevice applications.

RESULTS AND DISCUSSION

SWCNT Networks on Porous Silica. The porous silica layer was prepared from the silica sol with a particle size of about 15 nm, synthesized by the hydrolysis and condensation of tetraethyl orthosilicate (TEOS) in ethanol solvent. We then coated the porous silica layer onto the SiO_2/Si substrates using the dip-coating method, as reported previously.[25] In general, by using different starting solutions, we can prepare the porous silica layer with a range of thickness, pore size, porosity, and surface roughness (Supporting Information, Figure S1). Here two coatings were implemented, one was the thin layer with a thickness of ∼150 nm and the other was slightly thicker, ∼170 nm. X-ray photoelectron spectroscopy (XPS) analyses confirmed that the surface chemical composition of both coatings was indeed silica (Supporting Information, Figure S2). Atomic force microscopy (AFM) and field-emission scanning electron microscopy (FE-SEM) showed that the surfaces of both silica layers were of similar roughness and comprised many silica nanospheres, which coagulated to form a porous template with a pore size of 20−30 nm and a porosity of ∼50% (Supporting Information, Figure S3). The prepared substrates with porous layers as well as the uncoated SiO_2/Si substrates were then coated with thin Fe catalyst films to grow SWCNT networks. A "fast-heating" strategy was adopted to pretreat the catalysts,[26] followed by a reduction step in a coflow of Ar and H_2. After that, CH_4 was introduced as the carbon-containing precursor and SWCNTs were grown in an atmospheric-pressure CCVD. Further details can be found in the Methods section.

Figure 1 shows the FE-SEM images of the grown SWCNTs on all substrates. Apparently, one can see that the density of the nanotubes on these substrates is very different. The nanotube coverage is only ∼0.01 tubes/μm^2 on the uncoated surface but reaches 1−2 tubes/μm^2 on both the thin and thick porous silica-coated surfaces. Such a striking difference is clearly seen at the interface between the uncoated and thin silica-coated layers (Figure 1d and Supporting Information, Figure S4). Additionally, we noted that most of the nanotubes grown on the uncoated surface were short and straight, whereas they appeared much longer and curly on silica-coated surfaces. These longer nanotubes tended to form many "knots" in the networks, as pointed by arrows in Figure 1b,c. A quite similar morphology of SWCNTNs has also been observed previously using solution-based catalysts, where the evaporation of solution may redistribute the catalyst nanoparticles and form large aggregates before the actual growth of SWCNTs.[27,28] In contrast, a uniform catalyst thin film was used in the present work, facilitating the reproducibility and controllability of the networks. The effects of such "knotted" morphology on the nanoscale electronic transport will be discussed later.

Figure 2a shows typical resonant micro-Raman spectra of SWCNTs probed at both 514 and 633 nm laser excitations. While the radial-breathing mode (RBM) peaks and the tangential G peaks (at ∼1590 cm^{-1}) are

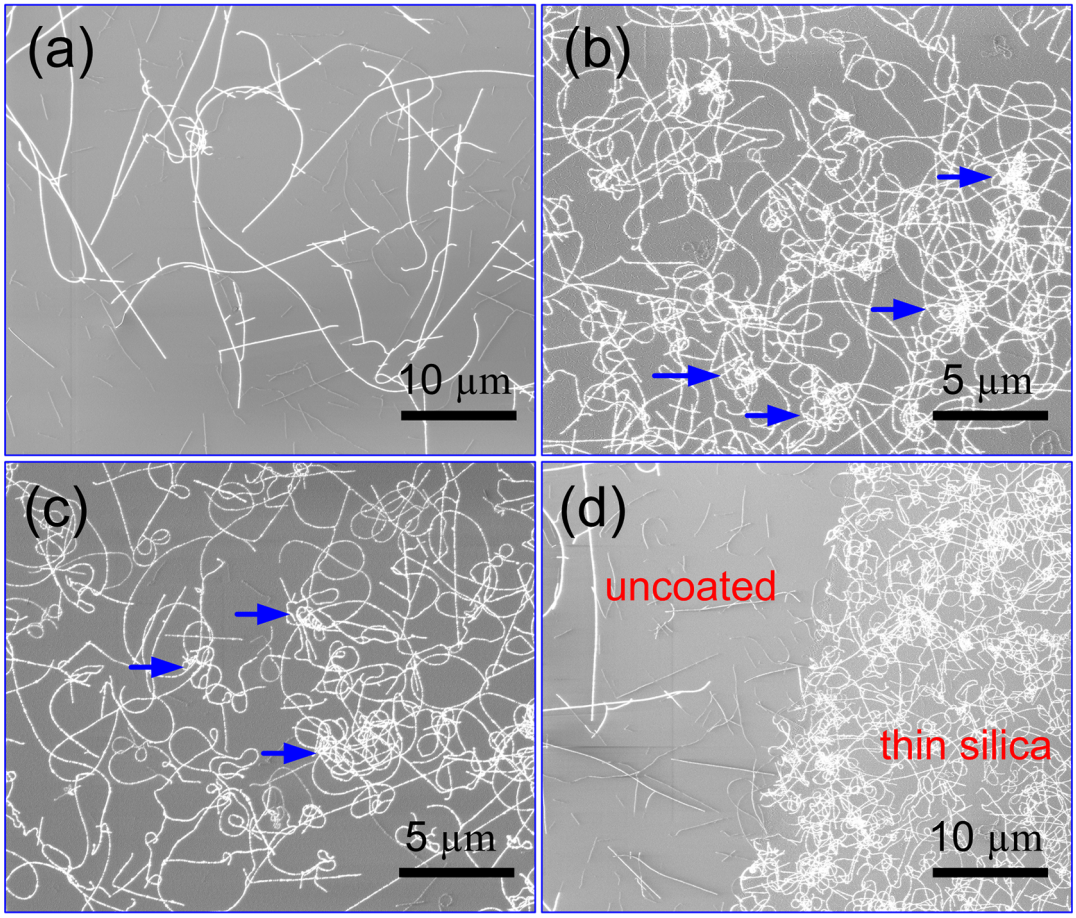

Figure 1. SWCNT networks grown on uncoated and porous silica-coated substrates. Nanotubes on (a) uncoated substrate show a much lower density than on (b) thin and (c) thick porous silica-coated substrates. Arrows in panels b and c indicate the special "knotted" morphology in the networks. The clear difference in the nanotube density at the interface of uncoated and thin silica-coated surfaces is also shown in panel d.

clearly shown as the characteristic features of SWCNTs, the disorder-associated D peaks (at ~1350 cm^{-1}) are almost indiscernible. The ratio of G/D intensities is commonly accepted as a crucial parameter in determining the purity and structural quality of the SWCNTs. In the present work, the G/D value (>50, with a very low D intensity) is among the highest values reported in the literature, indicating a very high quality of the grown nanotubes.[29] As compared to other hydrocarbon (*e.g.*, C_2H_4, C_2H_2) or alcohol precursors, CH_4 is thermally stable at high temperatures.[30] The catalytic decomposition of CH_4 therefore dominated over self-pyrolysis, effectively limiting the deposition of amorphous carbon.[31] The high-quality SWCNT growth in our experiments can be attributed to the optimized growth conditions. In particular, under conditions of the balanced supply of CH_4 and H_2, amorphous carbon can be effectively etched, and eventually, a structural defect-free growth (*e.g.*, without pentagonal or heptagonal carbon rings) can be achieved.[32]

We then patterned the Au electrodes on the surface of SWCNT networks and measured the sheet resistance using a two-point electrical probe configuration (Figure 2b and Supporting Information, Figure S5). The resistance is found to be the largest on the uncoated surface, followed by the thin silica-coated surface, and the lowest on the thick silica-coated surface, in a good agreement with their respective nanotube densities (Figure 2c). Furthermore, the current–voltage (I–V) curves of all three networks are shown in Figure 2d. One can see from this figure that while the I–V curve is nonlinear on the uncoated surface, they are almost linear on the porous silica-coated surfaces.

It is known that in single nanotube-based devices, a significant Schottky barrier can form at the nanotube–metal contact junction.[33] However, when many nanotubes are embedded in the metal electrode and a macroscopic contact is established, as in the case of the SWCNT networks, the contact resistance becomes very small as compared to the sheet resistance.[13,34] The main contribution in our electrical measurements is thus from the nanotube–nanotube junctions inside the networks.[12,35] The linearity of the I–V curves (ohmic behavior) observed on the porous silica-coated substrates indicates that the nanotube–nanotube

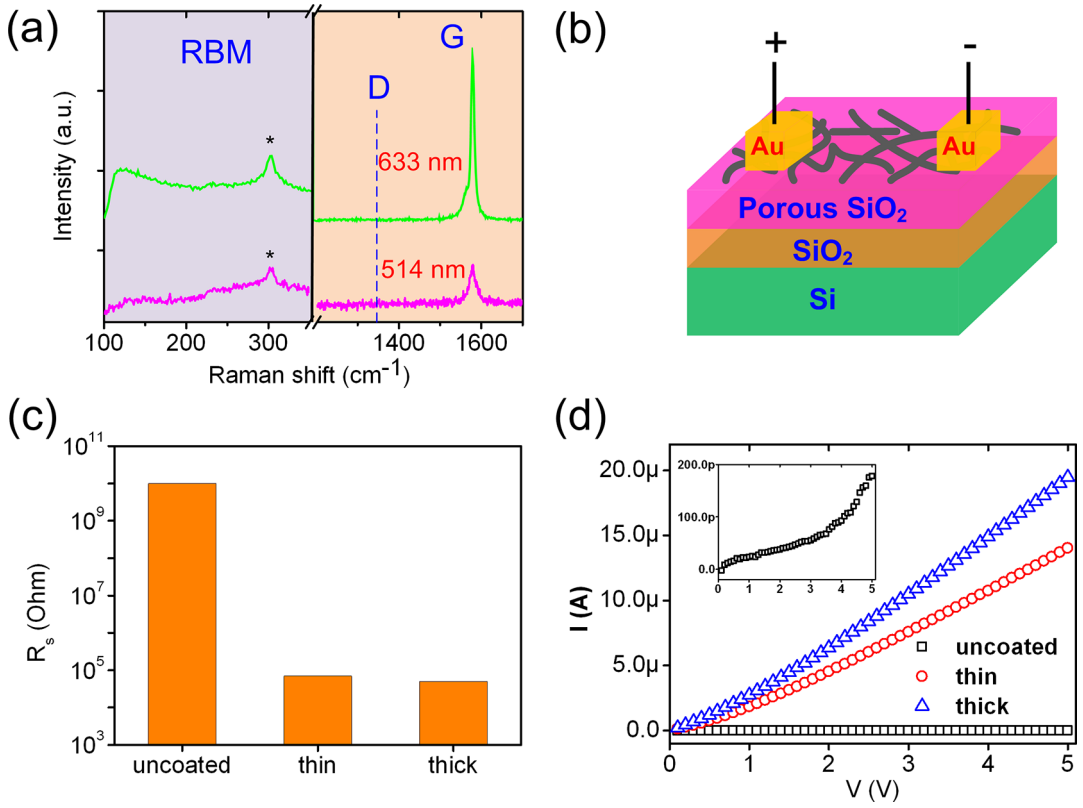

Figure 2. Properties of the SWCNT networks. (a) Typical Raman spectra of the nanotubes grown on the thin silica-coated substrate probed at 514 and 633 nm laser excitations. Very strong G-peak and almost diminishing D-peak are observed. Asterisks (∗) in the radial-breathing mode (RBM) band denote the peaks from the porous silica. (b) A schematic diagram of the electrical measurement setup. (c) The sheet resistance and (d) the I−V curves of SWCNT networks grown on the uncoated, thin, and thick silica-coated substrates. Inset in panel d is the enlarged plot in the uncoated substrate case.

junction resistance is greatly reduced as compared to the samples with high Schottky barriers. We emphasize that such a clearly ohmic behavior has previously been found only in networks either made of a highly pure metallic SWCNTs or when the nanotube density is very high (>10 tubes/μm^2); in these cases a very small intertube junction resistance is expected.[36,37]

Recently, Sun *et al.* demonstrated that long (>10 μm) nanotubes connected in a Y-junction morphology showed a low resistance and a high carrier mobility.[14] In a similar manner, we conclude that *the "knotted" morphology*, as mentioned earlier, significantly contributed to a large junction area and a strong coupling of electronic carriers in the present networks.[12−14] These "knots" could therefore dramatically reduce the sheet resistance and result in the observed ohmic behavior. Indeed, the resistance of our SWCNT networks is almost 3 orders of magnitude lower compared to typical solution-processed networks with a similar density.[37−39] Interesting, this special "knotted" morphology was not found in the C_2H_2-assisted growth on a flat substrate, although the nanotube density is comparable in both cases.[21] Sun *et al.* showed that long nanotubes formed the Y-junctions only when collected on the porous membrane filter but not on the flat SiO_2/Si substrate.[14] Therefore, the nanoporous silica catalyst support in the current case has most likely enabled the formation of the observed "knotted" SWCNT morphology shown in Figure 1.

It is worth mentioning that in order for SWCNT networks to be useable in functional nanodevices, a nanotube density higher than the percolation threshold is required so that the electron transport across the networks could be effectively sensed and manipulated.[40] The percolation threshold defines the onset of conductive pathways formed in the networks. Using the stick model,[14] the percolation threshold of SWCNT networks is $\rho_{th} = 4.24^2/(\pi L_{CNT}^2)$, where L_{CNT} is the average length of the nanotubes. Analyzing the morphological features in Figure 1, we estimated ρ_{th} to be 0.06 tubes/μm^2 for the networks grown on the uncoated surface. This value is much higher than the actual nanotube density (~0.01 tubes/μm^2, Figure 1a). This indicates that no percolation pathway could be formed on the uncoated SiO_2 surface. On the other hand, ρ_{th} is only 0.01 tubes/μm^2 for the SWCNT networks on the porous silica-coated surfaces due to a larger L_{CNT}. As the observed nanotube density (1−2 tubes/μm^2) on these surfaces is almost 2 orders of magnitude larger than the percolation threshold, many percolation pathways are formed in the

networks. These estimates are in a good agreement with their respective electrical measurements (Figure 2c).

We emphasize that the nanotube density on the porous silica-coated substrates is within the desirable range of many functional devices, including flexible electronics, transparent conductive coatings, and electrochemical sensors. The optimized density of these devices is typically 0.5−3 tubes/μm^2.[39−44] Given the controllable density together with the high nanotube quality, the special "knotted" morphology, and the good connectivity at the nanoscale, the SWCNT networks produced on the porous silica support are highly promising for these applications. Additionally, our method of preparing the nanoporous silica layer is simple, inexpensive, and environmentally friendly as compared to other methods such as electrochemical etching.[45] The nanoporous silica support is also thermally stable and compatible with the current semiconductor technologies, in contrast to other nonsilicon materials (*e.g.*, Al_2O_3 and TiO_2). It has been used as a low-*k* dielectric material in electronic nanodevices and is scalable toward large-size wafers for multiplexed devices using the conventional techniques such as photolithographic patterning and plasma etching.[46] The next step in the direction is to improve control over the metallic-to-semiconducting nanotube ratio in the networks to further improve their electrical performance.[47−49]

Growth Model: Effects of Nanoporous Silica. To explain the significant roles the nanoporous silica layer played in the growth of SWCNTs, we propose a growth model which accounts for the unique interactions between the Fe catalyst nanoparticles and the porous support. It is generally assumed that the Fe catalyst nanoparticles are in a liquid state during the growth of SWCNTs in the CCVD process, although other catalysts (such as Al_2O_3, SiO_2, and nanodiamond) may remain in solid state at high temperatures.[50] The widely accepted growth model, based on the vapor−liquid−solid (VLS) mechanism proposed for the growth of semiconducting nanowires, states that the growth of SWCNTs includes three stages: the nucleation stage, the growth stage, and the termination stage.[21,22,51] At first, carbon-containing gas or its derivatives adsorb onto the catalyst or the substrate surfaces and dissociate into atomic or molecular carbon species; nucleation occurs as these carbon species diffuse into the catalyst nanoparticles, reach a supersaturated state, and then segregate from the surface of nanoparticles to form a nanotube cap;[52,53] subsequently, the growth of nanotubes is sustained by the continuous incorporation of carbon atoms *via* bulk and/or surface diffusions. From the VLS mechanism, it is implied that a larger number of active catalyst nanoparticles and a more effective carbon diffusion lead to higher nucleation densities and growth rates of the nanotubes.

Our model compares two different nucleation and growth scenarios on the flat and porous surfaces. First, in contrast to the flat surface, a porous surface could provide appropriate interactions (neither too strong nor too weak) to effectively restrict surface diffusion and decrease the catalyst nanoparticle (CNP) coalescence, a kinetic process that is detrimental to the growth of high-density patterns of thin single-walled carbon nanotubes.[54] This may lead to a higher density of catalytically active nanoparticles with a much narrower size distribution,[20,55] as illustrated in Figure 3a,b. Second, the porous support provides *an additional channel for carbon diffusion* to the catalyst nanoparticles supported by the porous surface. Owing to the porous structure, carbon-containing species can diffuse into the underneath support layer and reach the bottom surface of the catalyst nanoparticles, thereby delivering more precursors for the nucleation and growth of SWCNTs (Figure 3c,d). In contrast, carbon precursor species can only be delivered through the open surface area and perimeter of CNPs when the nanotubes are grown on the flat surface.[52]

Given the higher-density of catalyst nanoparticles, reduced coalescence rate, and the improved precursor delivery, the nucleation of carbon nanotubes can be greatly enhanced and the lifetime of catalyst nanoparticles can be prolonged. As expected, these effects result in high-density and morphologically controlled nanotubes grown on the porous silica surfaces, consistent with our experimental observations.

Results of Numerical Modeling. To corroborate the above growth model and further elaborate the numerous advantages of employing a nanoporous silica support, we have conducted a combinatorial, multiphase numerical modeling to reveal the effects of the surface conditions and the catalyst nanoparticle characteristics on the nucleation and growth of SWCNTs. This numerical modeling takes into consideration the building units (BU) production and transport to catalyst nanoparticles, energy and matter exchange on the nanoparticle surface, surface and bulk diffusion of carbon species, and catalyst nanoparticle saturation, followed by the bending of a graphene monolayer on the CNP surface (see insets in Figure 3).[56] The effects of the porous layer were quantified by accounting for the changed surface roughness (and hence, the contact angle) as well as by incorporating the additional delivery of carbon species to CNPs through the porous network sketched in the inset in Figure 3b (the associated carbon flux is denoted J_{BP}). Some of the most important parameters, including the energy barrier for nucleation (ΔH^*), detachment of the graphene layer (E_B), and the SWCNT growth rate at the initial stage of nanotube formation (H_C), are calculated and analyzed. For more details please refer to the Methods section and the Supporting Information.

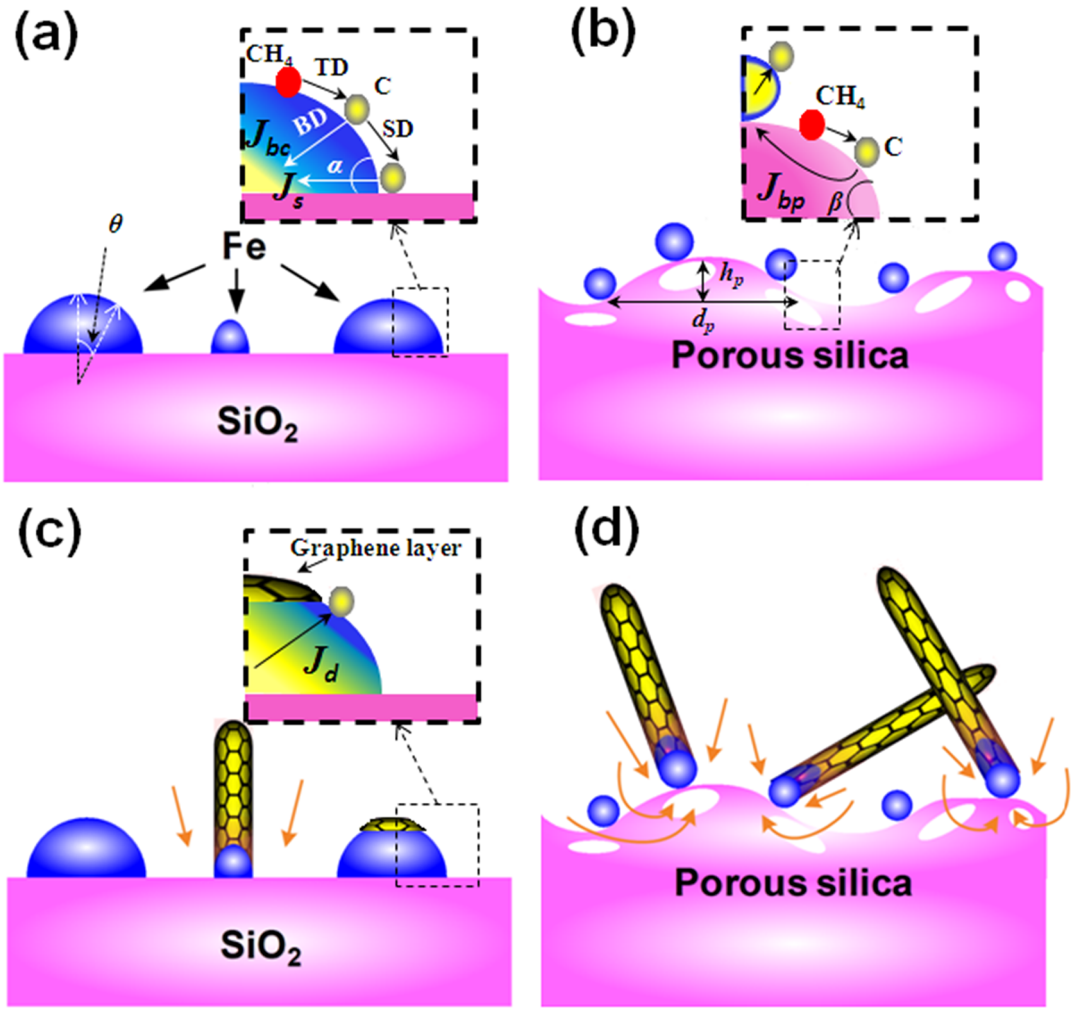

Figure 3. Illustrations of the roles of the porous silica layer in the growth of SWCNT networks. (a) Low-density catalyst nanoparticles with a wide size distribution are formed on the flat SiO_2 substrate; while (b) higher-density, narrowly distributed catalyst nanoparticles are formed on the porous silica layer. Insets in panels a and b show the surface and bulk diffusions of CH_4 species on the catalyst nanoparticles. They also include some of the most important processes in the nucleation and growth of SWCNTs, such as thermal dissociation of CH_4 (TD), bulk (BD), and surface diffusion (SD) of carbon atoms. (c) Limited gas supply on the flat SiO_2 substrate, as compared to (d) enhanced precursor diffusion from the porous silica layer. This results in a more effective nanotube nucleation, faster growth, and eventual reconnection of the nanotubes into a network as sketched in panel d. Inset in panel c illustrates the less effective detachment of a graphene layer from the large catalyst nanoparticle. See Methods and Supporting Information for more details.

The main results of numerical modeling are plotted in Figure 4, where the Fe catalyst radius is a variable in the range reported in our experiment. We have compared the growth on the flat Si (solid curve) and porous silica (dashed, dotted, and dash-dotted curves) layers to explain how the porous layer can promote the formation of denser and longer nanotube networks observed in our experiments. As one can see from Figure 4, the energy barrier for nucleation of a graphene layer (ΔH^*) is much smaller, while the bending energy for detachment of the graphene layer (E_B) and the SWCNT growth rate (H_C) become higher (in the considered range of CNP size), in the porous silica layer case as compared to the flat SiO_2 surface. These differences in the SWCNT nucleation and growth parameters are also more pronounced when the catalyst contact angle α becomes larger due to, for example, enhanced surface roughness (see also Supporting Information, Figure S8).[57]

The above modeling results can be explained by noting that a porous surface leads to a better saturation of the catalyst nanoparticles. The rough surface has a larger active area for the production of a larger number of the building units (carbon atoms) *via* thermal dissociation of precursor hydrocarbon species. Consequently, the energy barrier for the graphene layer formation (*i.e.*, the initial SWCNT cap formation) decreases, the bending of the graphene layer becomes more effective, and the growth rate increases. These factors eventually lead to the formation of much denser and longer SWCNT networks.

Gas and Biomolecular Sensing Applications. One of the most attractive applications of the random SWCNT networks is in gas and biomolecular sensing, which is

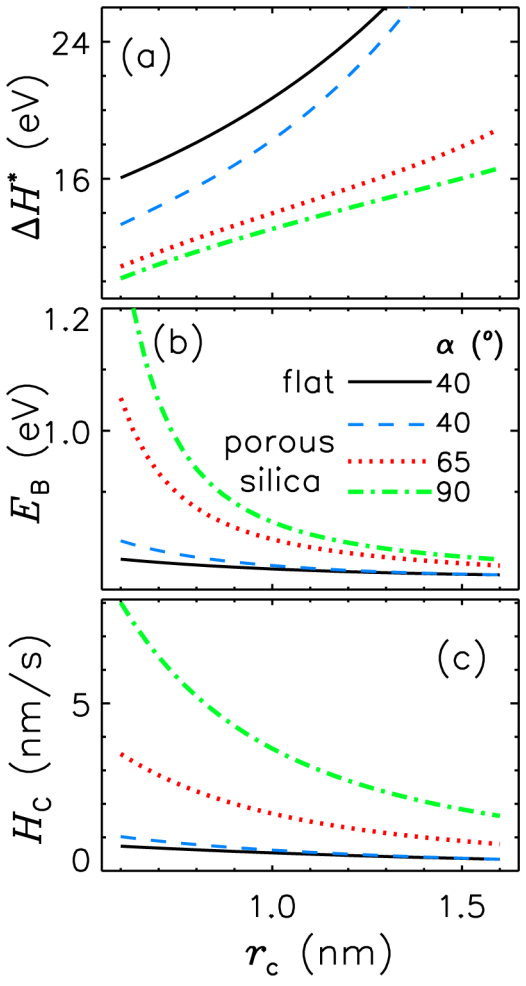

Figure 4. Numerical modeling results on the nucleation and growth of SWCNTs on both flat and porous surfaces. (a) The energy barrier for SWCNT nucleation (ΔH^*), (b) the bending energy for detachment of a graphene layer (E_B), and (c) the nanotube growth rate (H_C), are plotted as a function of the catalyst nanoparticle radius. The cases of both flat SiO_2 (solid curve) and porous silica (dashed and dotted, and dash-dotted curves) surfaces are considered. The dashed, dotted, and dash-dotted curves in panels a–c correspond to contact angles α of 40°, 65°, and 90°, respectively (see Methods and Supporting Information for more details).

closely related to environmental monitoring, medical diagnosis and therapy, public security, and a variety of industries.[58] Because of their large surface-to-volume ratio (essentially mostly surface atoms) which provides a greater adsorptive capacity and extremely high sensitivity of electronic properties (*e.g.*, conductance, capacitance) to the external environment,[3] SWCNTs are the ideal candidates for achieving a highly sensitive and rapid detection of gas and biomolecular analytes of interest, ranging from toxic chemical vapors to cancer biomarkers. In addition, compared to individual nanotubes, SWCNT networks can have a large number of tubes exposed to analytes simultaneously, which not only improve the signal-to-noise ratio and thus the detection limit, but also conveniently build large-scale sensing platforms for multiplexed detection.[59]

To demonstrate such applicability of the present SWCNT networks synthesized with the nanoporous silica supporting layer, we have fabricated a simple gas sensing device based on the chemiresistor configuration.[58] Briefly, two electrical contacts were deposited on the sample surface to act as source and drain; a resistor (10 kΩ) was connected in series with the sample to limit the current. When exposed to different gases, the changes in resistance were evaluated as the response of the SWCNT networks. Details on the device fabrication and the sensing experiments are given in the Methods section.

Figure 5a plots the room-temperature response of the sensor device to NH_3. One can see that when exposed to 0.5 ppm level of NH_3 in nitrogen, a clear increase in resistance could be observed. As the concentration of NH_3 was adjusted to 5 ppm, the resistance was significantly increased by about 7% within a relatively short time (~300 s). The resistance was further increased by 12% and 19% when 50 and 500 ppm NH_3 were injected, respectively. A fairly good recovery to the baseline resistance was followed after the cutoff of NH_3 supply in all exposures.

We previously demonstrated that the CNT yarns, which were formed by a bundle of small-diameter multiwalled carbon nanotubes (MWCNTs) twisted into a diameter between 20 to 40 μm, had a maximum NH_3 response of only 1–2% in their pristine form.[60] The sensitivity obtained in the current device was about 1 order of magnitude higher than that of the CNT yarns, and was comparable to that of field-effect transistor (FET)-based sensors based on individual SWCNTs (*e.g.*, a 25% reduction in conductance was observed within 300 s when exposed to 10,000 ppm NH_3).[61] Such a high sensitivity and good recovery of NH_3 were plausibly attributed to the optimized density and the good two-dimensional nanoscale connectivity, as demonstrated in the above structural and electrical analyses (see section SWCNT Networks on Porous Silica). In addition, the underneath nanoporous silica support might have also contributed to a better gas diffusion for detection during the sensing experiments.

Figure 5b plots the room temperature response of the sensor device when exposed to NO_2. Unlike in the case of NH_3, the resistance of SWCNT networks decreased very significantly. This is consistent with the charge transfer mechanism, where in the *p*-type SWCNT networks, the electron-withdrawing molecules (*e.g.*, NO_2) would increase the charge carrier density (holes) and the electron-donating molecules (*e.g.*, NH_3) would decrease the charge carrier density.[61] The responses have reached ~7%, ~32%, 41%, and 46% for the exposures of NO_2 for 0.5, 5, 50, and 500 ppm levels, respectively. An even higher response of ~65% could be obtained if the sensor was exposed to 500 ppm NO_2

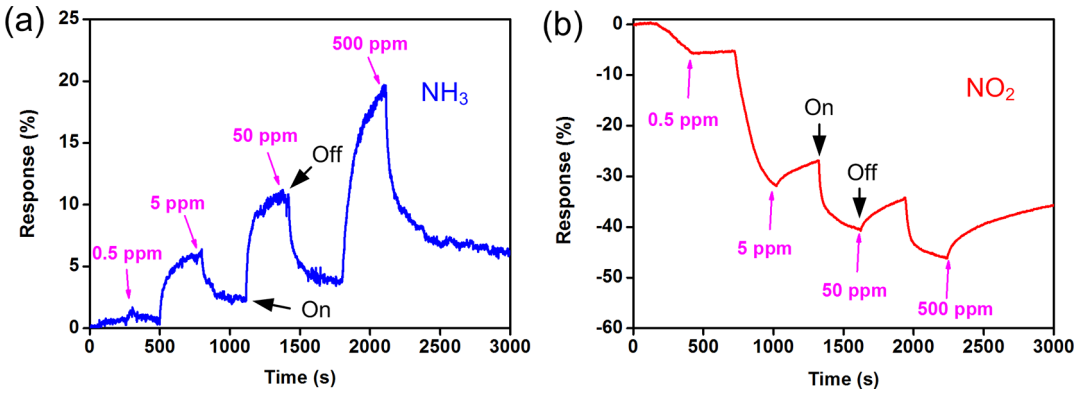

Figure 5. Performance of gas sensor devices based on the SWCNT networks grown with the nanoporous silica support layer. The sensor was sequentially exposed to 0.5−500 ppm (ppm) levels of (a) NH_3 and (b) NO_2 in nitrogen. At each cycle, the gas exposure time was set at 300 s, after which the gas was cutoff and 100% nitrogen was let into the chamber for another 300 s. "On" and "Off" are shown for just one curve but are similar for all four curves. The responses were calculated as the changes in resistance with respect to the original value.

at the beginning (Supporting Information, Figure S6). The recovery of the resistance in the cycles of NO_2 was typically slow, possibly due to the strong binding energy of NO_2 on SWCNTs (~0.8 eV) which impeded the desorption of NO_2 from the CNTs after the sensor was exposed to pure nitrogen atmosphere.[58]

Finally, we used the same device to detect the prostate specific antigen (PSA), a biomarker for prostate cancer. The SWCNTs used were in their pristine form without being functionalized by acid or antibody. We dispersed the solutions containing PSA molecules at different concentrations on the SWCNT networks and applied a constant voltage (1 V) across the source and the drain. In general, a clear trend in the reduction of the current (*i.e.*, an increase in resistance) was observed along with the increased concentration of PSA (Supporting Information, Figure S7). This is likely caused by the PSA molecules nonspecifically bound to the surface of SWCNTs due to hydrophobic interactions, $\pi-\pi$ stacking, or possibly amino-affinity of SWCNTs.[3] As a result, the conductivity of the sensor device was altered by the charge transfer of PSA molecules and the SWCNTs themselves functioned as labels for the reliable detection of PSA.

It should be noted that the above sensing results were obtained by incorporating the pristine SWCNT networks. We also expected that through further scaling down the size of the sensors (Supporting Information, Figure S6), decorating the SWCNTs with metal (such as Pd, Au) nanoparticles, or fabricating the interdigitated electrodes (IDEs), the sensitivity of both gases and biomolecules could be enhanced and the recovery profile could be improved.[62,63] Nevertheless, the current results clearly demonstrate the great promise of the SWCNT networks with a tailored density and nanoscale connectivity, which could be easily realized by incorporating nanoporous silica as the catalyst supporting layer in the CCVD growth process.

CONCLUSIONS

Prior to integrating the SWCNT networks into high-performance functional devices, one has to meet specific criteria: the density of the nanotubes in the networks should exceed the percolation threshold and be easily variable within the desirable range; the nanotubes should be of a very high structural quality; no amorphous carbon contamination should be found on the SWCNT walls; the electron scattering and Schottky barriers arising from the nanotube−nanotube and nanotube−metal junctions should be minimized.

We have successfully solved these problems by directly synthesizing the SWCNT networks using nanoporous silica layers for Fe catalyst nanoparticle support. The technique of coating the nanoporous silica layers was simple, inexpensive, and environmentally friendly. The silica layer was thermally stable as the catalyst support and compatible with the current semiconductor technologies. Our results revealed the transition from separated individual nanotubes to the interconnected networks, thereby heralding the achievement of the effective morphological and connectivity control at the nanoscale. High-quality nanotubes with the special "knotted" network morphology also enabled the dramatically reduced electrical sheet resistance. Moreover, the electrical measurements showed the clearly Ohmic behavior which is normally observed in networks of much higher density or networks made of high-purity metallic SWCNTs. Using a multiscale, multiphase numerical modeling, we have confirmed that the unique surface conditions on the porous silica and the increased carbon supply through the porous structure led to denser and longer SWCNTs. Further, simple sensing devices based on the SWCNT networks were fabricated, and their excellent performance on detecting a variety of gases and biomolecules was demonstrated. These results provide a simple, yet very effective method to enable effective

control over the density, morphology, and connectivity in SWCNT networks and better understand the effects of catalyst supports on the SWCNT nucleation and growth, which are important for various advanced nanoelectronics, energy conversion, and sensing applications.

METHODS

Nanoporous Silica Layer. Several methods have been available in the past for the preparation of nanoporous silica layer, for example, by electrochemical etching.[45,64,65] Here we used a simple sol−gel technique. The details of our method can be found in a previous publication.[25] Briefly, the silica sol with the particle size of about 20 nm was first synthesized by the hydrolysis and condensation of TEOS in ethanol (EtOH) solvent. The molar ratio of TEOS/EtOH/NH_3/H_2O used here was 1.0:38:0.54:2.0. Half of the EtOH was mixed with TEOS and the other half was mixed with ammonia and water and the two solutions were stirred for 15 min. After that, the solution with ammonia was dropwise added (with stirring) into the TEOS solution. Finally, the solution was allowed to stand at room temperature for a minimum of three days to become a silica sol. We then coated the silica sol on SiO_2/Si substrates with different thicknesses using the dip-coating method. Depending on the different molar ratio of the starting solutions, it was possible to adjust the porous silica layer with different thickness (50−300 nm), pore size (5−50 nm), porosity, and surface roughness (Supporting Information, Figure S1). In this work, two coatings were prepared, one was the thin layer with a thickness of ∼150 nm and the other was slightly thicker, ∼170 nm, as measured by ellipsometry (J. A. Woollam, VASE). The root-mean-square (rms) surface roughness of the two coated surfaces was similar and confirmed by the AFM measurements. The rms surface roughness was 1.97 and 2.04 nm for the thin and thick silica coatings, respectively.

CCVD Growth of SWCNT Networks. The prepared substrates were coated with a 0.5 nm thick Fe catalyst thin film by magnetron sputtering (AJA International Co.). The deposition rate was kept low (∼0.01 nm/s) and the substrate was rotated in order to maintain a uniform coating over a relatively large substrate area. The preparation of this catalyst system was similar to the spin-on-catalyst (SOC) and the wet Fe−alumina systems reported previously.[22,23] The catalysts were then loaded into a quartz tube furnace to grow the SWCNT networks.[21,47] In a typical CCVD process, a "fast-heating" technique was adopted to pretreat the catalysts. A 2-in. quartz tube was preheated to the desirable temperature (T = 900 °C), and then the catalysts were inserted into the tube center where a zone of ∼20 cm had a uniform and stable temperature. As soon as the catalysts were inserted, the quartz tube was evacuated to $\sim 10^{-1}$ Torr within 2 min by a rotary pump. Ar (200 sccm) and H_2 (200 sccm) were then introduced into the tube and the pressure was adjusted to 760 Torr using a throttle valve between the tube and the rotary pump. After 5 min, CH_4 was added into the Ar/H_2 flow to start the growth of SWCNTs, while the pressure was maintained at 760 Torr by the throttle valve. Finally, the growth was terminated after 10 min by switching off the CH_4 and H_2 gases, and the samples were cooled down to room temperature under a continuous Ar flow.

Characterization, Microanalysis, And Electrical Measurements. The field-emission scanning electron microscopy (FE-SEM; Zeiss Ultra Plus) used 1 keV electron acceleration energy and an InLens secondary electron detector. The working distance of high-resolution images was about 2.8 mm. The atomic force microscopy (AFM; Asylum Research MFP-3D) was operated in a tapping mode with an Al-coated monolithic silicon probe (Budget Sensors) which had a force constant of ∼5 N/m and a resonant frequency of ∼130 kHz. The resonant micro-Raman spectroscopy (Renishaw *inVia*) had a laser spot of ∼1 μm^2 and two laser excitations at 514 nm (Ar laser) and 633 nm (He−Ne laser) wavelengths. X-ray photoelectron spectroscopy (XPS; Specs SAGE 150) used the Mg Kα excitation at 1253.6 eV. In addition, transmission electron microscopy (TEM; Philips CM120) used 120 keV electron acceleration energy. Samples for TEM observations were prepared by scratching them from the substrate surface followed by dispersion in ethanol, which was then dropped on a holey carbon-coated copper grid (SPI Supplies) and dried in air.

The Au electrodes deposited on the surface of SWCNT networks were patterned by photolithography. The mask pattern had a channel width of 20 μm and a channel length of 100 μm. After photoresist (S1813, Shipley) deposition, UV exposure, and development, 50 nm thick Au was deposited by magnetron sputtering (AJA International, Inc.). Photoresist was then removed in acetone and the FE-SEM image showed that the density of the nanotubes was unchanged after these steps (Supporting Information, Figure S5). The sheet resistance and I−V curves were then measured by a semiconductor device analyzer (Agilent B1500A) at room temperature. The sheet resistance was ∼7.5 GΩ/□, 67 kΩ/□, and 50 kΩ/□ for the networks on uncoated, thin, and thick nanoporous silica-coated surfaces, respectively.

Numerical Modeling. We consider the Fe catalyst-assisted nucleation of SWCNTs on both porous silica and flat Si/SiO_2 layers exposed to Ar+H_2+CH_4 gas mixtures. The combinatorial model includes the species creation/loss, gas−surface-interaction, bulk diffusion, graphene layer nucleation, and bending/lift-off modules.[56] Insets in Figure 3a,b show the schematics of the prevailing thermal building unit creation and diffusion processes, such as thermal dissociation (TD), surface (SD), and bulk (BD) diffusion of the C species on/into the catalyst nanoparticle and porous layer surfaces (with angles α and β, respectively, and the surface temperature T = 900 °C used in the experiments), and the nucleation of the graphene layer (which will become the cap of the nanotube). Carbon atoms could diffuse into the catalyst directly *via* the catalyst bulk or indirectly by first diffusing through the bulk of porous layer and then into the nanoparticle (with fluxes J_{bc} and J_{bp} as sketched in Figure 3).

A higher concentration of carbon atoms in the catalyst FeC alloy increases the concentration of carbon atoms on the catalyst surface, which is favorable for the graphene layer nucleation, bending, and lift-off.[56] The porous silica layer reduces the coalescence rate of small Fe nanoparticles and leads to more effective CNP saturation, in part due to the much higher rates of TD of hydrocarbon precursors. This strong carbon flux along with a carbon flux from the porous layer could lead to more effective FeC alloy saturation and the effective segregation of a graphene layer. The set of default parameters are gas temperature T = 900 °C, gas pressure P_0 = 760 Torr, for the gas mixture of Ar(40%) + CH_4(30%) + H_2(30%). More details can be found in the Supporting Information.

Gas and Biosensing Devices. The as-grown SWCNT networks were first patterned with two gold electrodes by photolithography (Solitec) with a long channel length of 200 μm. Here the chemiresistor configuration was adopted with the two electrodes acting as source and drain. A resistor of 10 kΩ was also connected in series with the sample to limit the current. The sample was then mounted onto the testing unit using silver paste connecting the two gold electrodes and inserted into the gas sensing apparatus.[60] Dry nitrogen was used as the buffer gas. The resistance of the SWCNT networks was measured using a Keithley 2000 multimeter and the current limit was set as 10 μA to minimize Joule heating of the sample. When a stable baseline in resistance was established at the beginning, the sensor was sequentially exposed to cycles of either NH_3 or NO_2 at concentrations of 0.5, 5, 50, and 500 ppm. For each cycle, the gas exposure time was set at 300 s, after which the gas was

cutoff and 100% nitrogen was flown into the chamber for another 300 s (Figure 5). Responses were calculated as the changes in resistance with respect to the original baseline, that is, $(R - R_0)/R_0$, where R is the measured resistance upon exposure and R_0 is the resistance at baseline.

The same device was used for the detection of prostate specific antigen (PSA) molecules. The chemiresistor configuration was again adopted. The PSA was diluted in deionized water instead of the common phosphate buffer solution (PBS) to avoid the shunt resistance of the PBS solution and increase the sensitivity.[11] No anti-PSA antibody was preincubated on the device; instead, the pristine SWCNTs were used as the direct label for the detection of PSA. A drop (10 mL) of the PSA solution was dispersed on the surface. The circuit current was measured at different concentrations of PSA (varied from 75 nM to 7.5 mM) by applying a constant voltage across the source and drain (1 V).

Conflict of Interest: The authors declare no competing financial interest.

Acknowledgment. We thank S. Kumar, S. Yick, J. I. Wong, and W. Yan for technical assistance and fruitful discussions. Z.J.H. acknowledges CSIRO for the OCE Postdoctoral Fellowship. H.M. acknowledges support by the University of Sydney International Scholarship and CSIRO OCE top-up Scholarship. This work was supported by the Australian Research Council (ARC) and CSIRO's OCE Science Leadership Program.

Supporting Information Available: Representative silica coatings with different structure and morphology, chemical composition of the nanoporous silica layer, surface morphology of nanoporous silica layers used in the present work, FE-SEM images of SWCNT networks, electrical measurement setup, additional sensing results and devices, PSA sensing results, additional results on the effects of the increased contact angle of catalyst nanoparticles on nanoporous silica support, details of numerical modeling, and additional numerical results on SWCNT nucleation and growth. This material is available free of charge *via* the Internet at http://pubs.acs.org.

REFERENCES AND NOTES

1. Dai, H. Carbon Nanotubes: Synthesis, Integration, and Properties. *Acc. Chem. Res.* **2002**, *35*, 1035–1044.
2. Snow, E. S.; Novak, J. P.; Campbell, P. M.; Park, D. Random Networks of Carbon Nanotubes as an Electronic Material. *Appl. Phys. Lett.* **2003**, *82*, 2145–2147.
3. Cao, Q.; Rogers, J. A. Ultrathin Films of Single-Walled Carbon Nanotubes for Electronics and Sensors: A Review of Fundamental and Applied Aspects. *Adv. Mater.* **2009**, *21*, 29–53.
4. Hu, L.; Hecht, D. S.; Gruner, G. Percolation in Transparent and Conducting Carbon Nanotube Networks. *Nano Lett.* **2004**, *4*, 2513–2517.
5. Cao, Q.; Rogers, J. A. Random Networks and Aligned Arrays of Single-Walled Carbon Nanotubes for Electronic Device Applications. *Nano Res.* **2008**, *1*, 259–272.
6. Han, Z. J.; Ostrikov, K. Controlled Electronic Transport in Single-Walled Carbon Nanotube Networks: Selecting Electron Hopping and Chemical Doping Mechanisms. *Appl. Phys. Lett.* **2010**, *96*, 233115.
7. Li, H.; Loke, W. K.; Zhang, Q.; Yoon, S. F. Physical Device Modeling of Carbon Nanotube/GaAs Photovoltaic Cells. *Appl. Phys. Lett.* **2010**, *96*, 043501.
8. Hatakeyama, R.; Li, Y. F.; Kato, T. Y.; Kaneko, T. Infrared Photovoltaic Solar Cells Based on C_{60} Fullerene Encapsulated Single-Walled Carbon Nanotubes. *Appl. Phys. Lett.* **2010**, *97*, 013104.
9. Okimoto, H.; Takenobu, T.; Yanagi, K.; Miyata, Y.; Shimotani, H.; Kataura, H.; Iwasa, Y. Tunable Carbon Nanotube Thin-Film Transistors Produced Exclusively *via* Inkjet Printing. *Adv. Mater.* **2010**, *22*, 3981–3986.
10. Ishikawa, F. N.; Chang, H.-K.; Ryu, K.; Chen, P.-C.; Badmaev, A.; De Arco, L. G.; Shen, G.; Zhou, C. Transparent Electronics Based on Transfer Printed Aligned Carbon Nanotubes on Rigid and Flexible Substrates. *ACS Nano* **2009**, *3*, 73–79.
11. Lee, B. Y.; Sung, M. G.; Lee, J.; Baik, K. Y.; Kwon, Y.-K.; Lee, M.-S.; Hong, S. Universal Parameters for Carbon Nanotube Network-Based Sensors: Can Nanotube Sensors Be Reproducible? *ACS Nano* **2011**, *5*, 4373.
12. Nirmalraj, P. N.; Lyons, P. E.; De, S.; Coleman, J. N.; Boland, J. J. Electrical Connectivity in Single-Walled Carbon Nanotube Networks. *Nano Lett.* **2009**, *9*, 3890–3895.
13. Léonard, F.; Talin, A. A. Electrical Contacts to One- and Two-Dimensional Nanomaterials. *Nat. Nanotechnol.* **2011**, *6*, 773–783.
14. Sun, D.-M.; Timmermans, M. Y.; Tian, Y.; Nasibulin, A. G.; Kauppinen, E. I.; Kishimoto, S.; Mizutani, T.; Ohno, Y. Flexible High-Performance Carbon Nanotube Integrated Circuits. *Nat. Nanotechnol.* **2011**, *6*, 156–161.
15. Pereira, L. F. C.; Rocha, C. G.; Latgé, A.; Coleman, J. N.; Ferreira, M. S. Upper Bound for the Conductivity of Nanotube Networks. *Appl. Phys. Lett.* **2009**, *95*, 123106.
16. Moonoosawmy, K. R.; Kruse, P. To Dope or Not To Dope: The Effect of Sonicating Single-Wall Carbon Nanotubes in Common Laboratory Solvents on Their Electronic Structure. *J. Am. Chem. Soc.* **2008**, *130*, 13417–13424.
17. Kim, Y. L.; Jung, H. Y.; Kar, S.; Jung, Y. J. Cleaning Organized Single-Walled Carbon Nanotube Interconnect Structures for Reduced Interfacial Contact Resistance. *Carbon* **2011**, *49*, 2450–2458.
18. Fisher, C.; Han, Z. J.; Levchenko, I.; Ostrikov, K. Control of Dense Carbon Nanotube Arrays *via* Hierarchical Multilayer Catalyst. *Appl. Phys. Lett.* **2011**, *99*, 143104.
19. Li, Y.; Cui, R.; Ding, L.; Liu, Y.; Zhou, W.; Zhang, Y.; Jin, Z.; Peng, F.; Liu, J. How Catalysts Affect the Growth of Single-Walled Carbon Nanotubes on Substrates. *Adv. Mater.* **2010**, *22*, 1508–1515.
20. Seidel, R.; Duesberg, G. S.; Unger, E.; Graham, A. P.; Liebau, M.; Kreupl, F. Chemical Vapor Deposition Growth of Single-Walled Carbon Nanotubes at 600 °C and a Simple Growth Model. *J. Phys. Chem. B* **2004**, *108*, 1888–1893.
21. Han, Z. J.; Levchenko, I.; Yick, S.; Ostrikov, K. 3-Orders-of-Magnitude Density Control of Single-Walled Carbon Nanotube Networks by Maximizing Catalyst Activation and Dosing Carbon Supply. *Nanoscale* **2011**, *3*, 4848–4853.
22. Crouse, C. A.; Maruyama, B.; Colorado, R., Jr.; Back, T.; Barron, A. R. Growth, New Growth, and Amplification of Carbon Nanotubes as a Function of Catalyst Composition. *J. Am. Chem. Soc.* **2008**, *130*, 7946–7954.
23. Alvarez, N. T.; Hamilton, C. E.; Pint, C. L.; Orbaek, A.; Yao, J.; Frosinini, A. L.; Barron, A. R.; Tour, J. M.; Hauge, R. H. Wet Catalyst-Support Films for Production of Vertically Aligned Carbon Nanotubes. *ACS Appl. Mater. Interfaces* **2010**, *2*, 1851–1856.
24. de los Arcos, T.; Vonau, F.; Garnier, M. G.; Thommen, V.; Boyen, H.-G.; Oelhafen, P.; Duggelin, M.; Mathis, D.; Guggenheim, R. Influence of Iron−Silicon Interaction on the Growth of Carbon Nanotubes Produced by Chemical Vapor Deposition. *Appl. Phys. Lett.* **2002**, *80*, 2383–2385.
25. Li, X.; Shen, J. A Facile Two-Step Dipping Process Based on Two Silica Systems for a Superhydrophobic Surface. *Chem. Commun.* **2011**, *47*, 10761–10763.
26. Huang, S.; Woodson, M.; Smalley, R.; Liu, J. Growth Mechanism of Oriented Long Single Walled Carbon Nanotubes Using "Fast-Heating" Chemical Vapor Deposition Process. *Nano Lett.* **2004**, *4*, 1025–1028.
27. Zhang, H.; Wei, D.; Liu, Y.; Wu, B.; Huang, L.; Xi, H.; Chen, J.; Yu, G.; Kajiura, H.; Li, Y. A New ``Bones/Muscles'' Strategy for Preparing Highly Conducting Single-Walled Carbon-Nanotube Films with Ultrahigh Transparency. *Small* **2009**, *5*, 2392–2396.
28. Duong, B.; Seraphin, S.; Wang, L.; Peng, Y.; Xin, H. Production of Predominantly Semiconducting Double-Walled Carbon Nanotubes. *Carbon* **2011**, *49*, 3512–3521.
29. Ghorannevis, Z.; Kato, T.; Kaneko, T.; Hatakeyama, R. Narrow-Chirality Distributed Single-Walled Carbon Nanotube Growth from Nonmagnetic Catalyst. *J. Am. Chem. Soc.* **2010**, *132*, 9570–9572.

30. Kong, J.; Soh, H. T.; Cassell, A. M.; Quate, C. F.; Dai, H. Synthesis of Individual Single-Walled Carbon Nanotubes on Patterned Silicon Wafers. *Nature* **1998**, *395*, 878–881.
31. Kong, J.; Cassell, A. M.; Dai, H. Chemical Vapor Deposition of Methane for Single-Walled Carbon Nanotubes. *Chem. Phys. Lett.* **1998**, *292*, 567–574.
32. Teo, K. B. K.; Chhowalla, M.; Amaratunga, G. A. J.; Milne, W. I.; Hasko, D. G.; Pirio, G.; Legagneux, P.; Wyczisk, F.; Pribat, D. Uniform Patterned Growth of Carbon Nanotubes without Surface Carbon. *Appl. Phys. Lett.* **2001**, *79*, 1534–1536.
33. Appenzeller, J.; Lin, Y.-M.; Knoch, J.; Avouris, P. Band-to-Band Tunneling in Carbon Nanotube Field-Effect Transistors. *Phys. Rev. Lett.* **2004**, *93*, 196805.
34. Koechlin, C.; Maine, S.; Haidar, R.; Trétout, B.; Loiseau, A.; Pelouard, J.-L. Electrical Characterization of Devices Based on Carbon Nanotube Films. *Appl. Phys. Lett.* **2010**, *96*, 103501.
35. Blackburn, J. L.; Barnes, T. M.; Beard, M. C.; Kim, Y.-H.; Tenent, R. C.; McDonald, T. J.; To, B.; Coutts, T. J.; Heben, M. J. Transparent Conductive Single-Walled Carbon Nanotube Networks with Precisely Tunable Ratios of Semiconducting and Metallic Nanotubes. *ACS Nano* **2008**, *2*, 1266–1274.
36. Skákalová, V.; Kaiser, A. B.; Woo, Y.-S.; Roth, S. Electronic Transport in Carbon Nanotubes: From Individual Nanotubes to Thin and Thick Networks. *Phys. Rev. B* **2006**, *74*, 085403.
37. Asada, Y.; Miyata, Y.; Ohno, Y.; Kitaura, R.; Sugai, T.; Mizutani, T.; Shinohara, H. High-Performance Thin-Film Transistors with DNA-Assisted Solution Processing of Isolated Single-Walled Carbon Nanotubes. *Adv. Mater.* **2010**, *22*, 2698–2701.
38. Najeeb, C. K.; Lee, J.-H.; Chang, J.; Kim, J.-H. The Effect of Surface Modifications of Carbon Nanotubes on the Electrical Properties of Inkjet-Printed SWNT/PEDOT−PSS Composite Line Patterns. *Nanotechnology* **2010**, *21*, 385303.
39. Timmermans, M. Y.; Grigoras, K.; Nasibulin, A. G.; Hurskainen, V.; Franssila, S.; Ermolov, V.; Kauppinen, E. I. Lithography-Free Fabrication of Carbon Nanotube Network Transistors. *Nanotechnology* **2011**, *22*, 065303.
40. Sangwan, V. K.; Behnam, A.; Ballarotto, V. W.; Fuhrer, M. S.; Ural, A.; Williams, E. D. Optimizing Transistor Performance of Percolating Carbon Nanotube Networks. *Appl. Phys. Lett.* **2010**, *97*, 043111.
41. Liu, Y.; Jin, Z.; Wang, J.; Cui, R.; Sun, H.; Peng, F.; Wei, L.; Wang, Z.; Liang, X.; Peng, L.; Li, Y. Nitrogen-Doped Single-Walled Carbon Nanotubes Grown on Substrates: Evidence for Framework Doping and Their Enhanced Properties. *Adv. Funct. Mater.* **2011**, *21*, 986–992.
42. Ha, M.; Xia, Y.; Green, A. A.; Zhang, W.; Renn, M. J.; Kim, C. H.; Hersam, M. C.; Frisbie, C. D. Printed, Sub-3V Digital Circuits on Plastic from Aqueous Carbon Nanotube Inks. *ACS Nano* **2010**, *4*, 4388–4395.
43. Kim, S.; Kim, S.; Park, J.; Ju, S.; Mohammadi, S. Fully Transparent Pixel Circuits Driven by Random Network Carbon Nanotube Transistor Circuitry. *ACS Nano* **2010**, *4*, 2994–2998.
44. Cao, Q.; Kim, H.-s.; Pimparkar, N.; Kulkarni, J. P.; Wang, C.; Shim, M.; Roy, K.; Alam, M. A.; Rogers, J. A. Medium-Scale Carbon Nanotube Thin-Film Integrated Circuits on Flexible Plastic Substrates. *Nature* **2008**, *454*, 495–500.
45. Lee, T. J.; Seo, J.; Lee, H.; Lee, J. W.; Yi, W. Fabrication of Single-Walled Carbon Nanotube Three-Dimensional Networks Inside the Pores of a Porous Silicon Structure. *Carbon* **2010**, *48*, 1473–1479.
46. Huang, L.; Wind, S. J.; O'Brien, S. P. Controlled Growth of Single-Walled Carbon Nanotubes from an Ordered Mesoporous Silica Template. *Nano Lett.* **2003**, *3*, 299–303.
47. Han, Z. J.; Yick, S.; Levchenko, I.; Tam, E.; Yajadda, M. M. A.; Kumar, S.; Martin, P. J.; Furman, S.; Ostrikov, K. Controlled Synthesis of a Large Fraction of Metallic Single-Walled Carbon Nanotube and Semiconducting Carbon Nanowire Networks. *Nanoscale* **2011**, *3*, 3214–3220.
48. Neyts, E. C.; Shibuta, Y.; van Duin, A. C. T.; Bogaerts, A. Catalyzed Growth of Carbon Nanotube with Definable Chirality by Hybrid Molecular Dynamics-Force Biased Monte Carlo Simulations. *ACS Nano* **2010**, *4*, 6665–6672.
49. Neyts, E. C.; van Duin, A. C. T.; Bogaerts, A. Changing Chirality during Single-Walled Carbon Nanotube Growth: A Reactive Molecular Dynamics/Monte Carlo Study. *J. Am. Chem. Soc.* **2011**, *133*, 17225–17231.
50. Hong, G.; Chen, Y.; Li, P.; Zhang, J. Controlling the Growth of Single-Walled Carbon Nanotubes on Surfaces Using Metal and Non-metal Catalysts. *Carbon* **2012**, *50*, 2067–2082.
51. Qi, H.; Yuan, D.; Liu, J. Two-Stage Growth of Single-Walled Carbon Nanotubes. *J. Phys. Chem. C* **2007**, *111*, 6158–6160.
52. Noda, S.; Hasegawa, K.; Sugime, H.; Kakehi, K.; Zhang, Z.; Maruyama, S.; Yamaguchi, Y. Millimeter-Thick Single-Walled Carbon Nanotube Forests: Hidden Role of Catalyst Support. *Jpn. J. Appl. Phys.* **2007**, *46*, L399–L401.
53. Hofmann, S.; Blume, R.; Wirth, C. T.; Cantoro, M.; Sharma, R.; Ducati, C.; Havecker, M.; Zafeiratos, S.; Schnoerch, P.; Oestereich, A.; *et al.* State of Transition Metal Catalysts During Carbon Nanotube Growth. *J. Phys. Chem. C* **2009**, *113*, 1648–1656.
54. Amama, P. B.; Pint, C. L.; Kim, S. M.; McJilton, L.; Eyink, K. G.; Stach, E. A.; Hauge, R. H.; Maruyama, B. Influence of Alumina Type on the Evolution and Activity of Alumina-Supported Fe Catalysts in Single-Walled Carbon Nanotube Carpet Growth. *ACS Nano* **2010**, *4*, 895–904.
55. Lu, C.; Liu, J. Controlling the Diameter of Carbon Nanotubes in Chemical Vapor Deposition Method by Carbon Feeding. *J. Phys. Chem. B* **2006**, *110*, 20254–20257.
56. Ostrikov, K.; Mehdipour, H. Thin Single-Walled Carbon Nanotubes with Narrow Chirality Distribution: Constructive Interplay of Plasma and Gibbs-Thomson Effects. *ACS Nano* **2011**, *5*, 8372–8382.
57. Wang, Y.; Luo, Z.; Li, B.; Ho, P. S.; Yao, Z.; Shi, L.; Bryan, E. N.; Nemanich, R. J. Comparison Study of Catalyst Nanoparticle Formation and Carbon Nanotube Growth: Support Effect. *J. Appl. Phys.* **2007**, *101*, 124310.
58. Zhang, T.; Mubeen, S.; Myung, N. V.; Deshusses, M. A. Recent Progress in Carbon Nanotube-Based Gas Sensors. *Nanotechnology* **2008**, *19*, 332001.
59. Snow, E. S.; Novak, J. P.; Lay, M. D.; Perkins, F. K. 1/*f* Noise in Single-Walled Carbon Nanotube Devices. *Appl. Phys. Lett.* **2004**, *85*, 4172–4174.
60. Randeniya, L. K.; Martin, P. J.; Bendavid, A.; McDonnell, J. Ammonia Sensing Characteristics of Carbon-Nanotube Yarns Decorated with Nanocrystalline Gold. *Carbon* **2011**, *49*, 5265–5257.
61. Kong, J.; Franklin, N. R.; Zhou, C.; Chapline, M. G.; Peng, S.; Cho, K.; Dai, H. Nanotube Molecular Wires as Chemical Sensors. *Science* **2000**, *287*, 622–625.
62. Li, J.; Lu, Y.; Ye, Q.; Cinke, M.; Han, J.; Meyyappan, M. Carbon Nanotube Sensors for Gas and Organic Vapor Detection. *Nano Lett.* **2003**, *3*, 929–933.
63. Sun, Y.; Wang, H. H. High-Performance, Flexible Hydrogen Sensors That Use Carbon Nanotubes Decorated with Palladium Nanoparticles. *Adv. Mater.* **2007**, *19*, 2818–2823.
64. Wang, R.; Xu, H.; Guo, L.; Liang, J. Growth of Single-Walled Carbon Nanotubes on Porous Silicon. *Appl. Surf. Sci.* **2006**, *252*, 7347–7351.
65. Xu, Y.-Q.; Hauge, R. H. Growth of Single-Walled Carbon Nanotubes on a Nanorough Surface. *J. Phys. Chem. C* **2007**, *111*, 9142–9145.